Band model for the electronic structure of expanded liquid cesium

W. W. Warren, Jr. and L. F. Mattheiss

AT&T Bell Laboratories, Murray Hill, New Jersey 07974

(Received 26 March 1984)

Self-consistent, scalar-relativistic, linear-augmented-plane-wave calculations have been carried out for four (real and hypothetical) crystalline forms of cesium with the body-centered-cubic, simple-cubic, simple-tetragonal, and diamond structures at a fixed nearest-neighbor bond distance. The results of these calculations are applied to model the variation with density of several one-electron properties of expanded liquid cesium, including the total density of states $N(E_F)$, its $6s$ component $N_s(E_F)$, and the average Fermi-electron charge density at the nucleus. The calculations fail to explain an observed enhancement of the magnetic susceptibility at low densities. Also, contrary to experimental evidence derived from the combined analysis of Knight shift and susceptibility data, the calculated probability density at the nucleus for Fermi-surface electrons tends to increase rather than decrease as a function of decreasing density. This suggests that many-electron correlation effects play an essential role in determining the electronic properties of liquid cesium in the low-density limit where $\rho \lesssim 1.3$ g cm^{-3} and the nearest-neighbor coordination number $z \lesssim 6$.

I. INTRODUCTION

Liquid alkali metals can be expanded to densities that are about 20% of the normal solid or liquid density by heating to the liquid-gas critical point. Near the critical point they undergo a metal-nonmetal transition[1,2] resembling that proposed by Mott[3] in his original discussion of the metal-nonmetal transition in expanded monovalent crystals. At higher densities, in the metallic range, expanded liquid alkali metals offer a unique opportunity for experimental study of the effects of large density variations on the electronic properties of single-component monovalent systems.

A central question for the understanding of the electronic properties of expanded alkali metals, indeed, for the metal-nonmetal transition in general, is the role of electron-electron interactions. The Mott transition is itself a consequence of long-range Coulomb forces,[3] and Hubbard showed that the short-range intra-atomic Coulomb interaction can also lead to a metal-nonmetal transition.[4] Brinkman and Rice considered the role of the intra-atomic interaction in a metal and showed that the metallic state near the transition should be highly correlated, having a low instantaneous fraction of doubly occupied sites.[5] They predicted for this correlated metal an enhanced density of states (effective mass) and, consequently, enhanced values for the paramagnetic susceptibility and electronic specific heat.

The possible presence of large correlation effects in the alkali metals was first indicated by the magnetic susceptibility measurements for expanded liquid cesium reported by Freyland.[6] He observed an increasingly strong enhancement of the total mass susceptibility with decreasing density until a susceptibility peak was reached at about twice the critical density. Similar susceptibility enhancements have subsequently been observed in expanded liquid rubidium[7] and sodium.[8] Nuclear-magnetic-resonance measurements of the Knight shift[9] in Cs also

showed the low-density enhancement, confirming that the effect arises from the electron-spin contribution to the total susceptibility. Freyland[6] suggested that the enhancement was due to correlations, but there was little corroborating evidence. Recently[10] one of us has pointed out that the susceptibility peak is due to Curie law limitation of the susceptibility at low density, as might be expected for the density-of-states enhancement predicted by Brinkman and Rice.

The combined analysis[11] of these Knight shift[9] and susceptibility[6] data has provided additional information concerning the variation with density of the Fermi-electron charge density at the cesium nucleus, $\langle | \Psi(0) |^2 \rangle_{E_F}$. In particular, the ratio

$$\xi \equiv \langle | \Psi(0) |^2 \rangle_{E_F} / | \Psi(0) |^2_{\text{atom}} \tag{1}$$

is found to exhibit a surprising behavior in the low-density range. Instead of increasing toward the atomic limit $\xi = 1$, ξ assumes a roughly constant value of about 0.5 at high densities and then decreases rapidly when $\rho \lesssim 1.3$ g cm^{-3}. A qualitatively similar effect has also been observed for expanded liquid sodium although explicit values of ξ were not reported.[8]

In evaluating the possible role in these effects of electron-electron interactions, it is important to consider the predictions of one-electron theory for the electronic structure of an expanded alkali metal. One-electron theory has been highly successful in explaining the basic electronic properties of simple metals at ordinary densities and should provide a reference for interpreting the properties observed at low densities. In this paper we describe the use of self-consistent, scalar-relativistic, linear-augmented-plane-wave (LAPW) band calculations to model the electronic structure of expanded liquid cesium. The principal justification for the application of a band model to a liquid metal is the fact that many important features of electronic structure are determined largely by

local properties such as the number and distance of nearest neighbors. An experimental demonstration of this is the observation that most electronic properties of metals are only slightly affected by the loss of long-range order at the melting transition.

The simplest approach to modeling the low-density liquid is to assume an appropriate crystal structure with a variable lattice parameter. This approach has been followed by Rose,[12] Sander et al.,[13] and Kelly et al.,[14] who have carried out spin-density-functional calculations for bcc hydrogen and alkali metals as a function of the lattice parameter. One difficulty with this model is the intuitive expectation that it will yield a density-dependent ξ which increases more or less monotonically toward the atomic limit ($\xi = 1$) as the lattice parameter is increased.

The present investigation is based on an alternative structural model for the low-density liquid suggested by the neutron-diffraction data on expanded liquid rubidium.[15] It utilizes a series of crystal structures with decreasing numbers of nearest neighbors and a fixed nearest-neighbor bond distance.[16] An identical model was adopted in an earlier study of expanded liquid mercury.[17] Because of the added complexity introduced by the changes in both the crystal structure and nearest-neighbor coordination, it is more difficult to anticipate the variation of ξ or $N(E_F)$, the density of states at the Fermi energy, with decreasing density that is predicted by this model.

The principal results of our calculations include $N(E_F)$, its s-component $N_s(E_F)$, and the average Fermi-electron charge density at the nucleus. These results, when compared with empirical properties derived from susceptibility and Knight-shift data, show that the one-electron picture, as expected, works quite well at normal (high) density. However, the model fails to reproduce either the enhanced susceptibility or the decrease in ξ that is observed at low density, thus providing added support for the description of expanded cesium as a metal whose properties are strongly influenced by electron-electron interaction effects.

II. DETAILS OF THE CALCULATION

The structural model we have adopted for the present quasicrystalline treatment of expanded liquid cesium is suggested by the neutron-diffraction data on expanded liquid rubidium.[15] According to these results, a 50% density reduction in liquid rubidium is achieved primarily by a nearly linear decrease in the nearest-neighbor coordina-

tion number z and involves only a modest ($\sim 4\%$) increase in the nearest-neighbor bond distance b. In the present study, we neglect these small variations in b and assume that density changes are due solely to variations in the coordination number z.

The value for the nearest-neighbor bond distance $b = 5.31$ Å for liquid cesium has been determined from neutron-diffraction studies[18] at a temperature (~ 30 °C) just above the melting point. This study also yielded an average coordination number $z = 9.0 \pm 0.5$ for the normal liquid. It is interesting to note that this value for b in the liquid is identical to that for the solid at -10 °C,[19] where the structure is bcc and the coordination number $z = 8$. The lattice parameter for bcc cesium decreases by about 1.4% at low (~ 5 K) temperatures.[19]

The pertinent details of the crystal structures involved in our quasicrystalline treatment of expanded liquid cesium are summarized in Table I. As indicated, these structures include the stable bcc phase of the solid as well as a series of hypothetical forms of crystalline cesium with the simple-cubic (sc), simple-tetragonal (st), and diamond structures.

The simple-cubic and diamond structures are natural choices for modeling the sixfold and fourfold coordinated forms of the liquid because of their high symmetry and the fact that these structures are fully determined by the nearest-neighbor bond length b. The desirability of an alternative structural model for $z = 4$ is suggested by the results presented in the following section. In particular, it is found that the energy bands near E_F for cesium in the diamond structure are dominated by Brillouin-zone-boundary effects which eliminate most of the Fermi surface and yield a semimetal in which band overlap exists only on the hexagonal faces of the fcc Brillouin zone. Thus, in exception to the general rule, even gross features of the electronic structure near E_F for the diamond structure might differ significantly from the liquid, where the loss of long-range order would smear or even eliminate these boundaries entirely.

A reasonable alternative model for $z = 4$ is provided by the simple-tetragonal (st) structure with $c/a > 1$. In this case, the nearest-neighbor coordination is planar rather than tetrahedral. The c/a ratio has been arbitrarily set equal to 1.5 since this choice yields an atomic volume Ω which is close to that for the diamond structure and simplifies the density-of-states calculations described below. Because of the absence of specific zone-boundary effects the simple-tetragonal structure is more appropriate than the diamond structure, although the planar coordination

TABLE I. Summary of crystal structures and lattice parameters involved in the present quasicrystalline treatment of expanded liquid cesium, assuming a fixed nearest-neighbor bond distance $b = 5.31$ Å and a varying nearest-neighbor coordination number z.

	bcc [$Im3m$ (O_h^9)]	sc [$Pm3m$ (O_h^1)]	st [$P4/mmm$ (D_{4h}^1)]	diamond [$Fd3m$ (O_h^7)]
z	8	6	4	4
a (Å)	6.13	5.31	5.31	12.26
c (Å)			7.965	
Ω (Å³/atom)	115.26	149.72	224.58	230.51
ρ_{solid}(g cm⁻³)	1.92	1.47	0.98	0.96
ρ_{liquid}(g cm⁻³)	1.73	1.30	0.87	0.87

introduces some two-dimensional character which could not be expected in a real liquid.

The results in Table I also include values of ρ_{solid} and ρ_{liquid} for cesium at different coordination numbers z. The former values are calculated for a perfect single crystal of cesium with the indicated crystal structure and lattice parameters. The corresponding values for $\rho_{liquid}(z)$ have been estimated from the measured $\rho(z)$ values for liquid rubidium[15] by scaling with the density ratio of the two liquids at the melting point [$\rho(Rb)=1.47$ g cm^{-3}; $\rho(Cs)=1.84$ g cm^{-3}]. A comparison of ρ_{liquid} and ρ_{solid} indicates that the loss of long-range order in the liquid results in a 10—12 % decrease in the perfect-crystal values of $\rho_{solid}(z)$.

The present electronic-structure calculations for these various crystalline forms of cesium have been carried out with the use of a self-consistent, scalar-relativistic version[20] of the linear-augmented-plane-wave (LAPW) method.[21] In this scheme, the primitive unit cell is subdivided into nonoverlapping muffin-tin (MT) spheres centered at each atomic site and an interstitial region. Each LAPW basis function consists of a plane wave in the interstitial region which joins smoothly onto products of numerical radial functions times spherical harmonics within the MT spheres. The coefficients in the latter expansion are determined by matching the value and slope of the functions at the MT radii.

This method imposes no shape approximations on either the charge density or the potential. These functions are expanded in terms of lattice harmonics (radial functions times symmetry-determined linear combinations of spherical harmonics) within the MT spheres and a Fourier series in the interstitial region. The inclusion of nonspherical (MT) and nonconstant (interstitial) corrections to the crystalline charge density and potential becomes increasingly important in achieving high accuracy in calculations for structures with low coordination (i.e., the diamond and simple-tetragonal phases). The present formulation of the LAPW method employs a frozen-core approximation in which scalar-relativistic atomic charge densities are used to represent the cesium core ($\cdots 5s^2 5p^6$) states.

In the present calculations for each structure, the valence-band wave function for a particular wave vector $\vec{k}$ has been expanded in terms of a linear combination of LAPW basis functions with $(\vec{k}+\vec{G})^2 \leq 2.0-2.5$ a.u., where $\vec{G}$ is a reciprocal-lattice vector. This leads to a variational calculation for the energies and expansion coefficients involving approximately 60—70 LAPW's per cesium atom for each of the crystal structures involved. Based on past experience, this criterion is expected to yield energy eigenvalues which are converged to about 0.01 eV.

The MT sphere radii were set at the value $R \approx 2.63$ Å so that neighboring spheres nearly touched along the nearest-neighbor bond directions for each structure. The lattice harmonic expansion of the nonspherical contributions to the charge density and potential within the MT spheres included all terms through $l \leq 4$. The corresponding Fourier expansion of the charge density and potential in the interstitial region included about 400—600 plane waves per atom.

The self-consistent iterations were initiated by starting potentials derived from overlapping atomic charge densities. During each subsequent iteration cycle, the LAPW valence charge densities were evaluated by means of a uniform special-points sampling[22] of the appropriate Brillouin zones. For the bcc, sc, st, and diamond-structure calculations, the number of special points in the irreducible wedge of the Brillouin zone corresponded to 8, 10, 12, and 10 $\vec{k}$ values, respectively. These valence charge-density results were combined with those for the frozen core and applied to calculate an output crystal potential. In all calculations, the one-electron contribution to exchange and correlation effects have been treated in the local-density approximation using the Wigner interpolation formula.[23] (This exchange-correlation term is a one-electron rather than a many-electron effect;[3-6] it corrects the average one-electron coulomb potential to remove the interaction of an electron with itself.) The calculations converged rapidly to a self-consistent solution for each structure in which the average difference between the input and output potentials was about 0.001 eV and the energy eigenvalues exhibited even smaller variations.

Density-of-states curves have been calculated from the self-consistent LAPW results for each crystal structure with the use of the tetrahedral method.[24] These calculations have determined both the total density of states $N(E)$ as well as the angular-momentum projections $N_l(E)$. For the latter, the total density of states is weighted by the factor $f_l^{(n, \vec{k})}$, the integral over a MT sphere of the individual angular-momentum components of the LAPW charge density for the nth band at a given $\vec{k}$ point. Since this factor does not include the corresponding LAPW weight in the interstitial region, the sum over angular momenta, $f \equiv \sum_l f_l$, is less than 1 for valence-electron states.

The Brillouin-zone integrations involved in the density-of-states calculations for each structure have been carried out using a fairly coarse $\vec{k}$-space mesh involving 140, 84, 140, and 44 $\vec{k}$ points in the irreducible wedge of the bcc, sc, st, and fcc Brillouin zones, respectively. The mesh size Δk was chosen to subdivide the principal Brillouin-zone dimensions along k_x and k_y into six (sc, st, and diamond structures) or 12 (bcc structure) subunits. The choice $c/a=1.5$ in the st calculation allows an identical mesh size along k_z with four Δk subdivisions. To simplify the diamond-structure $N(E)$ calculations, the tetrahedral integrations were extended beyond the hexagonal face of the fcc-type Brillouin zone so as to include a sc-type wedge with twice the volume. The normalization of the final results was adjusted accordingly.

The use of a fairly coarse $\vec{k}$-space mesh in these $N(E)$ calculations is consistent with the present application because it tends to smear out fine-structure details in $N(E)$ which often arise from critical points near the Brillouin-zone boundaries. The density-of-states results presented in the following section have been further smoothed by convoluting the tetrahedral results with a Gaussian function having a full width at half maximum (FWHM) of 0.1 eV.
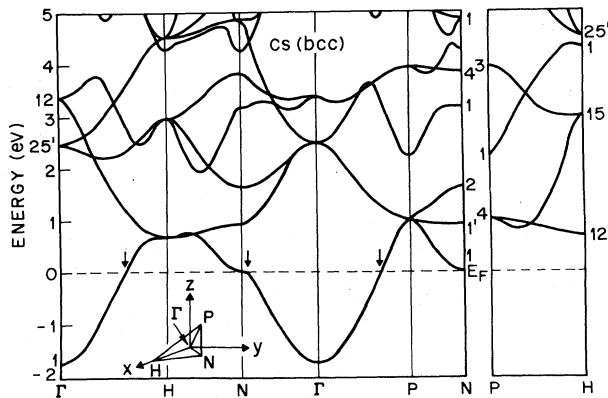
FIG. 1. LAPW energy-band results for bcc cesium along symmetry lines in the Brillouin zone (inset). The arrows denote Fermi radii derived from de Haas—van Alphen data (Ref. 26).

III. RESULTS

The present LAPW energy-band results for bcc cesium are shown in Fig. 1, where $E(\vec{k})$ is plotted along symmetry lines of the Brillouin zone (inset). As known from previous calculations,[25] the unoccupied conduction bands of the heavier alkali metals are dominated by the presence of d bands above the Fermi energy E_F. In Fig. 1 these extend roughly from the H_{12} to the $H_{25'}$ states

The bands near E_F are relatively isotropic and yield a nearly-spherical Fermi surface. The arrows indicate empirical Fermi radii that have been derived from de Haas—van Alphen studies.[26] The measured value of k_F along the $\Gamma-N$ direction shows that the N_1 band is above E_F by about 0.05—0.10 eV. N_1 coincides with E_F in the present calculations. However, this 0.05—0.10 eV error corresponds to the estimated accuracy of the present Fermi-energy determination. The general features of these energy-band results are in excellent agreement with those obtained in more recent[27] as well as in earlier theoretical studies.[28]

The energy-band results in Fig. 2 trace the evolution of the cesium electronic structure near E_F as the coordination number z is decreased at fixed bond length. Energy-band results are plotted along symmetry lines of the appropriate Brillouin zones (see insets) for hypothetical forms of cesium with the simple-cubic ($z=6$), simple-tetragonal ($z=4$), and diamond ($z=4$) structures. The band labels in Fig. 2 specify the dominant angular-momentum component $f_l^{(n,\vec{k})}$ of the LAPW wave function within the MT spheres at symmetry points. Based on the band connectivity near E_F, one might expect increased s-p and s-d hybridization at E_F in the simple-cubic and simple-tetragonal structures in comparison with the diamond-structure results. This is confirmed by the projected density-of-states results that are described below.

It is evident that the energy-band results near E_F for diamond-structured cesium are dominated by Brillouin-zone-boundary effects. This is due primarily to the fact that the diamond primitive cell contains two atoms. This leads to a semimetallic-type band structure with limited
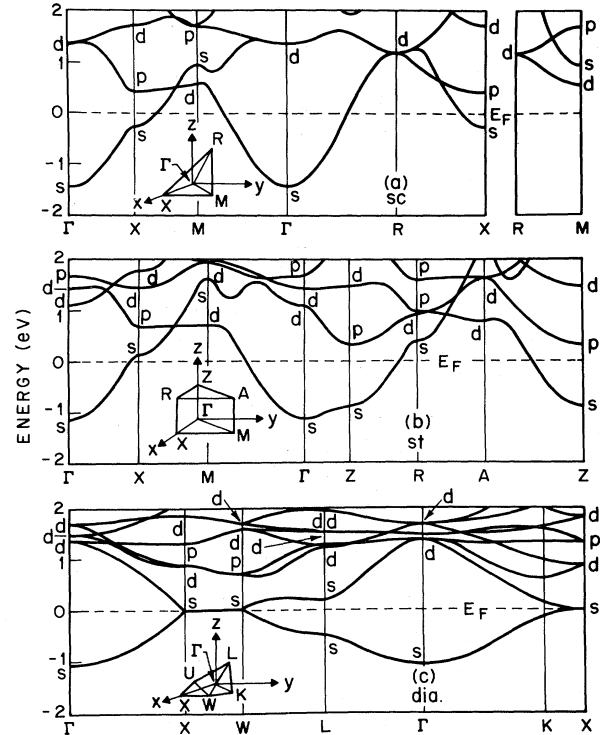

FIG. 2. LAPW results for hypothetical forms of crystalline cesium with the (a) simple-cubic, (b) simple-tetragonal, and (c) diamond structures. The dominant angular-momentum component f_l of the LAPW wave functions for individual bands at symmetry points (see insets) is indicated.

band overlap occurring only near the $X-W$ line on the surface of the Brillouin zone. These effects also produce a deep minimum in the density of states at E_F [see Fig. 3(c)]. Because of the fundamental relationship between the Brillouin-zone geometry and translational symmetry (i.e., long-range order), one can anticipate that the diamond-structure results may not be representative of those for a disordered fourfold-coordinated system. As mentioned in the preceding section, these considerations have led to the consideration of an alternate structural model for $z=4$, the simple-tetragonal structure.

These conclusions regarding the electronic-structure results near E_F for diamond-structure cesium are consistent with those of Joannopoulos and Cohen[29] who have modeled the electronic properties of amorphous Ge and Si by means of pseudopotential calculations on complex crystalline phases. According to their analysis, a specific feature of the diamond structure is responsible for the existence of the corresponding density-of-states minimum in the Ge and Si results, namely the presence of six-membered chair-shaped rings. Using arguments based on the distribution of molecular-orbital energy levels, they show that this density-of-states minimum is washed out when the local structural topology is modified to include either five- or seven-membered rings. In this context, it is interesting to note that stacking faults (which change the shape but not the size of these rings) have little effect on
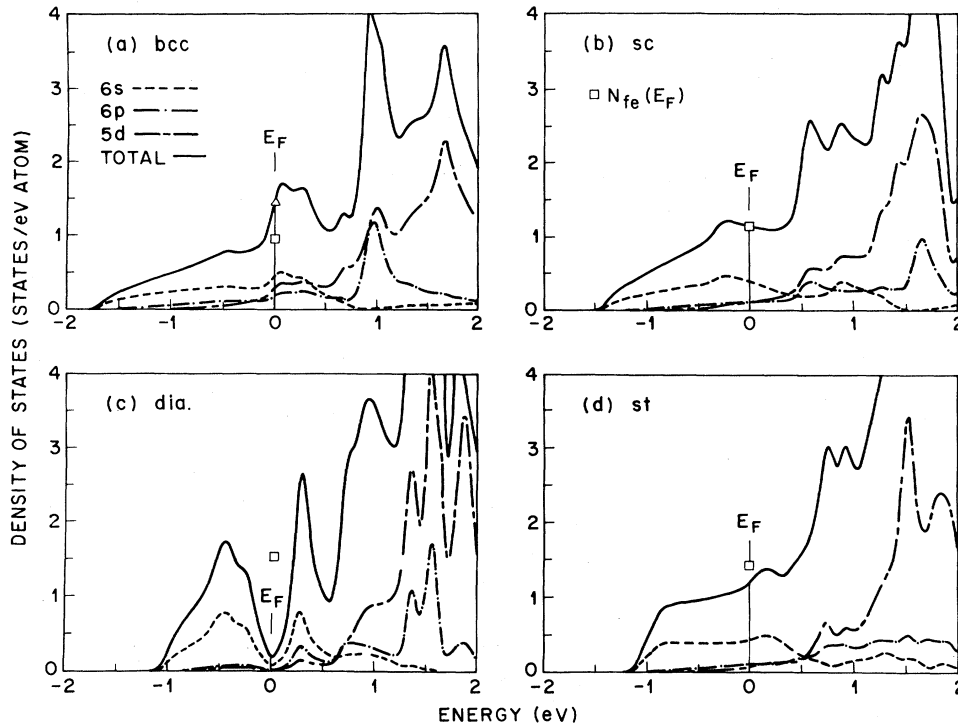
FIG. 3. Total $N(E)$ and projected $N_l(E)$ curves near E_F for cesium with the (a) bcc, (b) simple-cubic, (c) diamond, and (d) simple-tetragonal structures. The projected results are weighted by f_l, the integrated LAPW charge of angular momentum l within the MT spheres. The curves have been smoothed with a Gaussian function with FWHM of 0.1 eV. The free-electron values $N_{FE}(E_F)$ are shown by the square symbols. The triangle in (a) denotes the band-structure density of states that is derived from specific-heat data (corrected for electron-phonon enhancement effects, as discussed in the text).

the Si electronic structure in this energy range.[30]

Density-of-states curves for these various crystalline forms of cesium are shown in Fig. 3. As described in Sec. II, these results have been calculated by means of the tetrahedral method with the use of a fairly coarse $\vec{k}$-space grid to minimize peaks arising from critical points near the Brillouin-zone boundaries. The curves have been further smoothed with a Gaussian function with an 0.1-eV FWHM. The st $N(E)$ curve in Fig. 3(d) exhibits a step-like shape at low energies below the d band which is characteristic of that for a two-dimensional electron gas.

The dashed curves in Fig. 3 correspond to the various projected density-of-states results $N_l(E)$ ($l \leq 2$) in which the total density of states $N(E)$ is weighted by the factor f_l, the angular-momentum decomposition of the integrated LAPW charge within the MT spheres. Since these projections omit the corresponding LAPW weight in the interstitial region, the quantities f_l and N_l satisfy the relations $\sum_l f_l = f < 1$ and $\sum_l N_l(E) < N(E)$. The calculated values of these quantities at E_F for each crystal structure are presented in Table II.

The general features of the bcc $N(E)$ and $N_l(E)$ results are in good overall agreement with those obtained in previous energy-band studies.[27,31] The resolution of the $N(E)$ and $N_l(E)$ curves calculated by Jan et al.[27] is particularly high. This permits one to identify those minor features in Fig. 3(a) that are artifacts of the coarse Brillouin-zone integration mesh and energy smoothing. We note that the weight f_l of the linear-muffin-tin-orbital wave function[27] is normalized over the unit cell

($\sum_l f_l = 1$) so that the sum of the angular-momentum projections yields $\sum_l N_l = N$.

The triangle in Fig. 3(a) denotes the observed band-structure value for $N(E_F)$ that is derived from heat-capacity data[32] for bcc cesium, using Grimvall's estimate[33] that the electron-phonon enhancement factor $(1+\lambda) \approx 1.15$ in this material. The agreement with the calculated curve is excellent. Also shown by the square symbols in Fig. 3 are the free-electron values of the density of states at E_F, $N_{FE}(E_F)$. The observed value of $N(E_F)$ is clearly in better agreement with the LAPW result than that predicted by a free-electron model.

Another electronic property that is important for interpreting the Knight shift in expanded liquid cesium is the Fermi-electron probability density at the nucleus, $\langle |\Psi(0)|^2 \rangle_{E_F}$. In the nonrelativistic limit, only s electrons have finite charge density at the nucleus so that the Fermi-surface average involves only the s component, $|\Psi_s(0)|^2$. In the fully relativistic Dirac theory, both the $s_{1/2}$ and $p_{1/2}$ functions have charge densities at the nucleus, though the latter are reduced by a factor of order $\alpha^2 Z^2$, where $\alpha \approx 1/137$ is the fine-structure constant.[34] The present scalar-relativistic wave functions represent an average of the $j = l \pm \frac{1}{2}$ components[35] and do not include this feature of fully relativistic $p_{1/2}$ wave functions. We estimate that these corrections amount to about 15% for cesium ($Z = 55$).

The evaluation of $|\Psi_s(0)|^2$ in both the scalar-relativistic and Dirac models is further complicated by a weak though integrable divergence in the $s_{1/2}$ charge den-

TABLE II. Summary of calculated electronic properties at E_F for cesium as a function of crystal structure and coordination (z). The results include the free-electron and LAPW values for the density of states N_{FE} and N, respectively, the integrated charge in the MT sphere f, the square of the $6s$ component of the LAPW wave function near the nucleus $\langle\,|\,\Psi_s(r_1)\,|^2\rangle_{E_F}$, and its ratio to the atomic value ξ. The projected density-of-states values $N_l(E_f)$ are calculated by weighting N with the corresponding f_l's.

	Structure (z)			
	bcc (8)	sc (6)	st (4)	diamond (4)
$N_{FE}(E_F)$[a]	0.97	1.16	1.52	1.55
$N(E_F)$[a]	1.58	1.13	1.23	0.18
$N_s(E_F)$	0.48	0.38	0.44	0.07
$N_p(E_F)$	0.19	0.12	0.11	0.02
$N_d(E_F)$	0.32	0.10	0.08	0.01
f	0.64	0.54	0.51	0.54
f_s	0.31	0.34	0.36	0.41
f_p	0.12	0.11	0.09	0.09
f_d	0.20	0.09	0.06	0.05
$\langle\,|\,\Psi_s(r_1)\,|^2\rangle_{E_F}$[b]	5.21	5.92	6.03	7.12
ξ[c]	0.68	0.78	0.79	0.94

[a]In units states/eV atom.
[b]In units (a.u.)$^{-3}$, where $r_1 \approx 1.14 \times 10^{-4}$ a.u.
[c]$\xi \equiv \langle\,|\,\Psi_s(r_1)\,|^2\rangle_{E_F}/|\,\Psi_s(r_1)\,|^2_{atom}$, where $|\,\Psi_s(r_1)\,|^2_{atom} = 7.61$ (a.u.)$^{-3}$.

sity at $r=0$ for a point nucleus.[34] As a result, one must assume a model for the nucleus in order to calculate this quantity directly. To avoid this complication, we approximate $|\,\Psi_s(0)\,|^2$ by $|\,\Psi_s(r_1)\,|^2$, where $r_1 \approx 1.14 \times 10^{-4}$ a.u. coincides with the estimated radius of the cesium nucleus.

In calculating $\langle\,|\,\Psi_s(r_1)^2\,|\,\rangle_{E_F}$ for each structure, we have included in the Fermi-surface average selected $\vec{k}$ points from the density-of-states mesh for which the band energies fall in the range $E=E_F\pm0.2$ eV. This average over a finite-energy shell near E_F was introduced as a means for modeling the expected band-structure and Fermi-surface smearing in the liquid state. It had no significant influence on the results.

In each calculation, approximately, 15 $\vec{k}$ points in the irreducible Brillouin-zone wedge were included in this averaging procedure. The results of this calculation are included in the lower portion of Table II. This table also contains values for the parameter ξ evaluated from the approximation to Eq. (1):

$$\xi \approx \langle\,|\,\Psi_s(r_1)\,|^2\rangle_{E_F}/|\,\Psi_s(r_1)\,|^2_{atom} , \tag{2}$$

where $|\,\Psi_s(r_1)\,|^2_{atom}$ is the scalar-relativistic $6s$ charge density at r_1 for the cesium atom. It is preferable to compare experimental and theoretical values of ξ since this allows cancellation of any systematic corrections to the theory that occur in both the atom and the solid.

A careful analysis of the results presented in Table II reveals an important relation between the values for ξ [or $\langle\,|\,\Psi_s(r_1)\,|^2\rangle_{E_F}$] and f_s, the integrated $6s$ charge density inside the MT spheres,

$$f_s \equiv \int_{sphere} \rho_s(\vec{r})dv . \tag{3}$$

To an accuracy of about 2%, ξ is proportional to f_s,

$$\xi \approx 2.24 f_s . \tag{4}$$

This result is perhaps not very surprising. It confirms the intuitive idea that $\rho_s(\vec{r}_1) \equiv |\,\Psi_s(\vec{r}_1)\,|^2$ near the nucleus should scale with the integral of $\rho_s(\vec{r})$ over the MT sphere.

We can obtain a better understanding of the tabulated values for ξ as a function of coordination in Table II by plotting $f_s(E)$ for each of the four structures. These results are shown in Fig. 4. The corresponding ξ values are indicated by the scale to the right, assuming that Eq. (4) is valid over the conduction-band energy range. It is interesting to note, for example, that the tendency for ξ to increase toward the atomic limit $(\xi\rightarrow1)$ as the coordination number z is reduced occurs only in an energy range
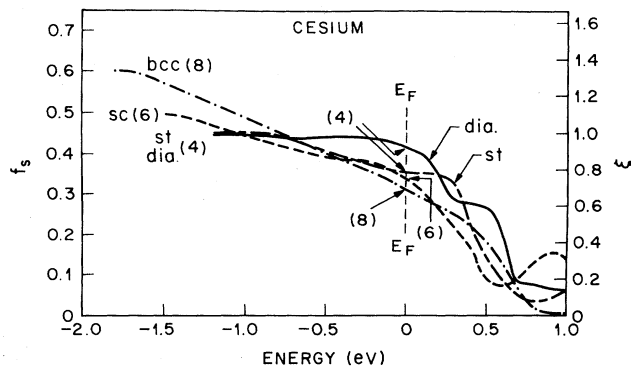

FIG. 4. Variation with coordination and energy of f_s, the $6s$ component of the LAPW wave functions within the MT spheres. The corresponding scale of ξ values shown to the right are derived with the use of Eq. (4).

near E_F. The opposite trend occurs for states near the bottom of the $6s$ conduction band, where ξ exceeds 1 for bcc-type coordination. Based on the shape of the $f_s(E)$ curves near E_f, one expects little effect from the energy averaging over ± 0.2 eV in the calculation of $\langle \,|\,\Psi_s(r_1)\,|^2\rangle_{E_F}$ for each structure.

We can compare the present calculated atomic charge density near the cesium nucleus $|\,\Psi_s(r_1)\,|^2_{\text{atom}} = 7.61$ (a.u.)$^{-3}$ with the value extracted from atomic-beam measurements,[36] where $|\,\Psi_s(0)\,|^2_{\text{atom}} = 3.81$ (a.u.)$^{-3}$. The source of this factor of 2 discrepancy is not fully understood, though it appears to be due to relativistic effects. For example, a similar but smaller discrepancy has been reported recently by Chermette,[37] whose scalar-relativistic calculations of $|\,\Psi_s(0)\,|^2_{\text{atom}}$ for cesium in the local-density approximation overestimate the measured value while the nonrelativistic results underestimate this quantity. Our atomic calculations carried out in the nonrelativistic limit $(c \rightarrow \infty)$ yield $|\,\Psi_s(r_1)\,|^2_{\text{atom}} = 2.77$ (a.u.)$^{-3}$, which is in reasonable agreement with the Herman-Skillman value,[38] ~ 2.5 (a.u.)$^{-3}$. However, these values are significantly larger than those derived from fully relativistic and nonrelativistic Hartree-Fock calculations, where $|\,\Psi_s(0)\,|^2_{\text{atom}} = 2.44$ and 1.63 (a.u.)$^{-3}$, respectively.[39]

IV. APPLICATION TO LIQUID CESIUM

A. Magnetic susceptibility

In this section we compare the predictions of our band model with the measured magnetic susceptibility of expanded liquid cesium. The susceptibility was measured by Freyland[6] along the liquid-gas coexistence curve over the density range $0.65 \lesssim \rho \lesssim 1.8$ g cm^{-3}. In order to compare our calculations with this result it is necessary to extract the electron-spin paramagnetic contribution $\chi^{e,p}$ from the total measured susceptibility χ_{tot}. We consider χ_{tot} to be the sum of three contributions

$$\chi_{\text{tot}} = \chi^{e,p} + \chi^{e,d} + \chi^{i,d} \,, \tag{5}$$

where $\chi^{e,d}$ is the diamagnetic susceptibility of the conduction electrons and $\chi^{i,d}$ is the diamagnetism of the Cs$^+$ ion cores. In terms of mass susceptibilities, $\chi^{i,d}$ is known[40] to be -0.263×10^{-6} cm^3 g^{-1} and $\chi^{e,d}$ can be calculated from the theory of Kanazawa and Matsudawa[41] for the electron gas. Their result is

$$\chi^{e,d} = -0.8629 r_s^{-1}[1 + 0.0276 r_s(\ln r_s + 1.51)]$$
$$\times \rho^{-1} \times 10^{-6} \text{ cm}^3 \text{ g}^{-1} \,, \tag{6}$$

where r_s is the mean electron radius $r_s = (3M/4\pi N_0 \rho)^{1/3}$ a.u., M is the atomic weight and N_0 is Avogadro's number. The results of this decomposition of $\chi^{e,p}$ for liquid Cs along the coexistence curve are plotted as a solid line in Fig. 5. As the density decreases from its maximum value at the melting point, the spin susceptibility initially decreases, then rises strongly to a peak near a density of 0.8 g cm^{-3}.

To calculate the mass susceptibility from our density-of-states results, we assume an enhancement of the Stoner form[42]
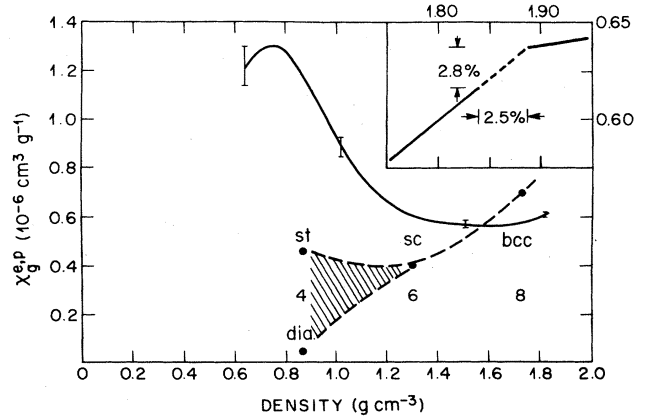

FIG. 5. Density dependence of the spin paramagnetic mass susceptibility $\chi_g^{e,p}$ for expanded liquid cesium along the coexistence curve. Solid line: experimental results of Ref. 6 decomposed as described in text. Solid dots: calculated susceptibility, enhanced according to Eq. (7), calculated from the LAPW density of states $N(E_F)$. Numerals indicate average coordination numbers. Inset: density dependence of $\chi_g^{e,p}$ in solid and liquid cesium near the melting transition (dashed line). Data are taken from Ref. 44 and normalized to those of Ref. 6 in the liquid range. Percentage changes of $\chi_g^{e,p}$ and density are indicated.

$$\chi_g^{e,p} = \frac{\mu_B^2 N(E_F)}{1-\alpha} \left[\frac{N_0}{M} \right] \,, \tag{7}$$

where μ_B is the Bohr magneton and $N(E_F)$ is the density of states per atom. The enhancement parameter α is the product $JN(E_F)$ of the density of states and the exchange-correlation integral J.

At a density of 1.73 g cm^{-3} corresponding to $z = 8$, we have $N(E_F) = 1.58$ (eV atom)$^{-1}$ from Table II. Nuclear magnetic relaxation and Knight-shift measurements[9] at this density yield $(1-\alpha)^{-1} \simeq 1.82$ so that $J \simeq 0.29$ eV. With these parameters, Eq. (7) yields $\chi_g^{e,p} = 0.70 \times 10^{-6}$ cm^3 g^{-1} which can be compared with the experimental value 0.575 ± 0.015 cm^3 g^{-1}. The discrepancy of about 22% is not unreasonable in light of uncertainties in the diamagnetic correction and the enhancement parameter and, of course, our use of a crystalline structure to model the liquid. In fact, this result shows that a one-electron band model provides a useful approach for approximating the electronic structure of the liquid at high density.

Similar calculations are done for the $z = 6$ and $z = 4$ coordination numbers to obtain the band-theory prediction for the density dependence of $\chi_g^{e,p}$. We assume a constant value $J = 0.29$ eV and obtain the results plotted in Fig. 5. It is clear that these one-electron results provide a poor description of the experimental curve at low density, predicting little or no increase in the susceptibility on passing from $z = 6$ to $z = 4$.

The band model does suggest a qualitative explanation for the initial decrease in $\chi_g^{e,p}$ that is observed at high density. The basic effect is due to a narrowing of the d bands as the coordination number z is reduced. As shown by

the z dependence of $N_d(E_F)$ and f_d in Table II, this causes a decrease in the average d character of the electron states at E_F as z varies from 8 to 4. This trend is consistent with the calculations of Yamashita and Asano[43] for compressed bcc and fcc cesium which predict a monatonic decrease in the d character at E_F as the lattice parameter is increased toward the equilibrium value.

Of course, another contributing factor to the large value of $N(E_F)$ for bcc cesium is the proximity of the N_1 state to E_F in Fig. 1. Since this Brillouin-zone-boundary N_1 state produces a sharp peak[27] in $N(E)$, it may be argued that this feature is an artifact of long-range order that will be substantially washed out by the effects of disorder in the liquid. However, an analysis of Collings data[44] for the susceptibility change of cesium at the melting transition shows that the change in $N(E_F)$ is exceedingly small. After correction for ionic and electronic diamagnetism, the data show that $\chi_g^{e,p}$ increases by only 2.8% at the melting transition (inset, Fig. 5).[45] This is thus a particularly clear demonstration of the insensitivity to long-range order of a feature of the electronic structure which differs significantly from the free-electron model. For cesium, the density dependence of $\chi_g^{e,p}$ across the transition is identical with that of the liquid just above the melting point; a weaker density dependence is observed for the solid as it is cooled under its own vapor pressure.

This discrepancy between one-electron theory and experiment at low density might, in principle, be reconciled by allowing the exchange-correlation integral to increase substantially. However, this is inconsistent with the measured nuclear relaxation rates[9] interpreted according to the Stoner model as it is usually applied to alkali metals at normal density. In fact, application of the conventional model to nuclear relaxation would require that J decrease substantially at low density.[9]

The resolution of this dilemma must be that the Stoner-enhanced one-electron picture breaks down at low density. The NMR data, for example, reveal significant changes in the q dependence of the susceptibility enhancement.[9] Deviations from the Korringa relation between the Knight shifts and nuclear relaxation rates provide a rough comparison of the high-q ($q \sim k_F$) enhancement with that at $q = 0$. Analyses of the data for cesium[9] and sodium[8] at low density show that the enhancement at high q increases relative to that at $q = 0$. This implies a trend toward antiferromagnetic enhancement, in contrast to the Stoner model which favors ferromagnetism (maximum enhancement at $q = 0$). Another aspect of the failure of Eq. (7) is the observation that the susceptibility is limited by the Curie value at low density. This is responsible for the peak in the experimental results for $\chi_g^{e,p}$ shown in Fig. 5.[10] There is no intrinsic limit to the Stoner enhancement of Eq. (7) and, in fact, near a transition to ferromagnetism, the susceptibility may greatly exceed the Curie value. On the other hand, a Curie susceptibility is expected if the density of states itself is enhanced as predicted, for example, for a highly correlated metal. As a result of a high density of states, the effective degeneracy temperature becomes comparable with the experimental temperature at the high temperatures necessary for study of expanded alkali metals.

B. Conduction electron wave functions

While the susceptibility provides an indication of the evolution of the density of states at E_F in the expanded metal, the Knight shift combined with susceptibility data reveals some features of the wave functions at low density.[11] The Knight shift may be written

$$K = \frac{8\pi}{3} \langle \, | \, \Psi \, | \, (0) \, | \,^2 \rangle_{E_F} \chi_g^{e,p} (M/N_0) \, , \tag{8}$$

where $\langle \, | \, \Psi(0) \, | \,^2 \rangle_{E_F}$ is the average probability density at the nucleus, averaged over states at the Fermi level. Using experimental values of K and the values of $\chi_g^{e,p}$ shown in Fig. 5, we have evaluated $\langle \, | \, \Psi(0) \, | \,^2 \rangle_{E_F}$ from Eq. (8). These values, normalized to the experimental atomic value[36] $| \, \Psi(0) \, | \,^2_{atom} = 3.81$ (a.u.)$^{-3}$ according to Eq. (1), are plotted in Fig. 6 for liquid cesium along the coexistence curve. As reported previously,[11] the result is that ξ is roughly independent of density ($\xi = 0.51 \pm 0.01$) at high density but, surprisingly, drops rapidly as the density decreases below about 1.3 g cm^{-3}. Since the low-density atomic limit corresponds to $\xi = 1$, one might have expected ξ to increase with decreasing density. Ultimately, of course, at some density below the current experimental range, ξ must again increase to the atomic value.

Our calculations of ξ from the band model given in Table II are compared with experiment in Fig. 6. At the
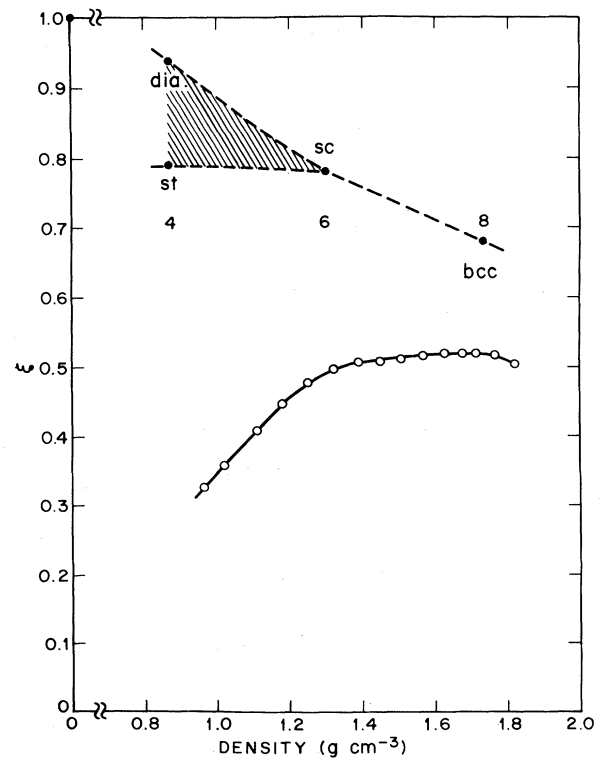

FIG. 6. Density dependence of the normalized charge density at the nucleus ξ for expanded liquid cesium along the coexistence curve. Open circles: experimental values (Ref. 11) derived from Knight shift (Ref. 9) and susceptibility (Ref. 6). Solid circles: theoretical values from LAPW calculations. Numerals indicate average coordination numbers.

highest density $(z=8)$, the theory overestimates ξ by about 30%. This discrepancy is of the same order as we found for the susceptibility and again indicates that the model is reasonably good for the high-density metal. However, the calculated trend for decreasing density is opposite to that of the experimental values and the overestimate grows to roughly a factor of 3 for $z=4$. Thus the theoretical result corresponds roughly to the intuitive expectation that ξ should increase toward the value $\xi=1$ for a pure atomic $6s$ state, while experiment shows that either the states are becoming less s-like at low density, which seems very unlikely, or charge is moving away from the atom and into the interstitial volume. Again, as we found for the susceptibility, the one-electron model fails badly in the low-density range.

C. Discussion: electron correlation and exchange at low density

We have shown that the one-electron band model at low density fails to account for the enhanced susceptibility, even including Stoner-type exchange-correlation enhancement, and the trend of the probability density at the nucleus. These indications of significant changes in the electronic structure must be considered in the light of three additional pieces of information: (i) the trend from ferromagnetic enhancement to antiferromagnetic enhancement of the wave-vector-dependent susceptibility $\chi(q)$; (ii) the inference of an enhanced density of states and reduced degeneracy temperature from the Curie limited susceptibility at the lowest densities; and (iii) theoretical predictions that the ground state of expanded atomic hydrogen and alkali metal crystals should be antiferromagnetic.[13,14]

The density dependence of the conduction-electron wave functions is qualitatively consistent with the implication of the magnetic properties that the short-range exchange interaction changes from ferromagnetic to antiferromagnetic at low densities. While a detailed description of this effect represents a difficult challenge for theory, the essential physics may be illustrated by consideration of the Heitler-London model for the hydrogen molecule. It is familiar result that the two-electron wave function $\Psi_\pm(\vec{r}_1, \vec{r}_2)$ may be represented by combinations of atomic functions $\phi_a(\vec{r})$ and $\phi_b(\vec{r})$ centered on atoms a and b, respectively, and spin functions $\chi_\pm$:

$$\Psi(\vec{r}_1, \vec{r}_2) = 1/[2(1\pm S^2)]^{1/2}[\phi_a(\vec{r}_1)\phi_b(\vec{r}_2)$$
$$\pm \phi_a(\vec{r}_2)\phi_b(\vec{r}_1)]\chi_\pm , \quad (9)$$

where the overlap factor is

$$S = \int \phi_a^*(\vec{r})\phi_b(\vec{r})d\vec{r} \quad (10)$$

and the $+$ and $-$ signs apply for the spin singlet and triplet functions, respectively. Use of the wave function of Eq. (9) to evaluate the charge density $\rho(0)$ at one of the

nuclei yields

$$\rho_\pm(0) = |\phi_a(0)|^2/(1\pm S^2) \quad (11)$$

Thus $\rho_+(0)/\rho_-(0) = (1-S^2)/(1+S^2)$ and the charge density at the nucleus is smaller for the singlet (antiferromagnetic) configuration than for the triplet (ferromagnetic). Correspondingly, more charge may be found between the atoms for the singlet configuration.

The observed trends in the electronic properties of expanded cesium mirror these elementary effects in the hydrogen molecule, i.e., a shift of electronic charge from the vicinity of the nucleus and antiferromagnetic-type exchange. Indeed, dense cesium vapor consists of atoms as well as diatomic molecules whose ground states are spin singlets.[6] In the expanded liquid with *average* coordination number 4, density fluctuations can be expected to lead to regions of significantly lower (and higher) local coordination. Thus it is perhaps not surprising to find indications of antiferromagnetic interaction in the low-density liquid.

V. CONCLUSIONS

In this paper we have applied LAPW band-structure results to describe the electronic structure of expanded liquid cesium. A structural model was assumed in which the average nearest-neighbor coordination number decreases in proportion to the density while the nearest-neighbor bond distance remains constant. The results show that the one-electron band picture is a good model for the high-density liquid, yielding reasonable results for the density of states at E_F and the electronic wave function at the nucleus. However, this one-electron model begins to fail at intermediate densities and ultimately provides a poor description of the low-density liquid metal.

We attribute the failure of the band model at low density not to inapplicability of the structural model, but to the dominant role of electron-electron interactions at low density. The observed physical properties, especially the enhanced susceptibility limited by the Curie law and indications of antiferromagnetic interactions, are consistent with the predictions of Brinkman and Rice for a highly correlated metal. The magnetic properties of expanded liquid cesium are essentially those of a nearly antiferromagnetic metal or an antiferromagnetic metal at a temperature well above its ordering temperature.

[1]H. Renkert, F. Hensel, and E. U. Franck, Ber. Bunsenges. Phys. Chem. **75**, 507 (1971).

[2]G. Franz, W. Freyland, and F. Hensel, J. Phys. (Paris) Colloq. **41**, C8-70 (1980).

[3]N. F. Mott, Proc. Phys. Soc. London, Sect. A **62**, 416 (1949).

[4]J. Hubbard, Proc. R. Soc. London, Ser. A **277**, 237 (1964); **281**, 401 (1964).

[5]W. F. Brinkman and T. M. Rice, Phys. Rev. B **2**, 4302 (1970).

[6]W. Freyland, Phys. Rev. B **20**, 5104 (1979).

[7]W. Freyland, J. Phys. (Paris) Colloq. **41**, C8-74 (1980).

[8]L. Bottyan, R. Dupree, and W. Freyland, J. Phys. F **13**, L173 (1983).

[9]U. El-Hanany, G. F. Brennert, and W. W. Warren, Jr., Phys. Rev. Lett. **50**, 540 (1983).

[10]W. W. Warren, Jr., Phys. Rev. B **29**, 7012 (1984).

[11]W. W. Warren, Jr., U. El-Hanany, and G. F. Brennert, in *Proceedings of the Fifth International Conference on Liquid and Amorphous Metals*, J. Non-Cryst. Solids **61-62**, 23 (1984).

[12]J. H. Rose, Phys. Rev. B **23**, 552 (1981).

[13]L. M. Sander, H. B. Shore, and J. H. Rose, Phys. Rev. B **24**, 4879 (1981).

[14]P. J. Kelly, T. M. Rice, O. K. Andersen, and D. Glötzel, Bull. Am. Phys. Soc. **27**, 322 (1982).

[15]G. Franz, W. Freyland, W. Gläser, F. Hensel, and E. Schneider, J. Phys. (Paris) Colloq. **41**, C8-194 (1980).

[16]A disordered version of this structural picture has been employed recently by Franz [J. R. Franz, Phys. Rev. B **29**, 1565 (1984)] in model calculations of $N(E)$ for expanded liquid cesium using a simplified (single-band, nearest-neighbor) tight-binding Hamiltonian. A random distribution of vacancies on the metal "lattice" was assumed.

[17]L. F. Mattheiss and W. W. Warren, Jr., Phys. Rev. B **16**, 624 (1977).

[18]N. S. Gingrich and L. Heaton, J. Chem. Phys. **34**, 873 (1961).

[19]W. B. Pearson, *A Handbook of Lattice Spacings and Structures of Metals and Alloys* (Pergamon, Oxford, 1964).

[20]D. R. Hamann, Phys. Rev. Lett. **46**, 1227 (1981); D. R. Hamann, L. F. Mattheiss, and H. S. Greenside, Phys. Rev. B **24**, 6151 (1981).

[21]O. K. Andersen, Phys. Rev. B **12**, 3060 (1975).

[22]H.-J. Monkhorst and J. D. Pack, Phys. Rev. **13**, 5188 (1976).

[23]E. Wigner, Phys. Rev. **46**, 1002 (1934).

[24]O. Jepsen and O. K. Andersen, Solid State Commun. **9**, 1763 (1971); G. Lehmann and M. Taut, Phys. Status Solidi B **54**, 469 (1972).

[25]F. S. Ham, Phys. Rev. **128**, 82 (1962).

[26]A. A. Gaertner and I. M. Templeton, J. Low Temp. Phys. **29**, 205 (1977).

[27]J.-P. Jan, A. H. MacDonald, and H. L. Skriver, Phys. Rev. B **21**, 5584 (1980).

[28]References to the more recent literature can be found in Ref. 26, while the earlier calculations are reviewed by Ham in Ref. 25 and M. J. G. Lee, CRC Crit. Rev. Solid State Sci. **2**, 85 (1971).

[29]J. D. Joannopoulos and M. L. Cohen, Phys. Rev. B **7**, 2644 (1973).

[30]L. F. Mattheiss and J. R. Patel, Phys. Rev. B **23**, 5384 (1981).

[31]E. A. Kmetko, in *Electronic Density of States,* edited by L. H. Bennett (Natl. Bur. Stand. (U.S.) Special Publication No. 323, Washington, D. C., 1971).

[32]D. L. Martin, Can. J. Phys. **48**, 1327 (1970).

[33]G. Grimvall, Phys. Scr. **14**, 63 (1976).

[34]H. Kopfermann, *Nuclear Moments* (Academic, New York, 1958).

[35]D. D. Koelling and B. N. Harmon, J. Phys. C **10**, 3107 (1977); H. Gollisch and L. Fritsche, Phys. Status Solidi B **86**, 145 (1978); J. H. Wood and A. M. Boring, Phys. Rev. B **18**, 2701 (1968).

[36]P. Kusch and H. Taub, Phys. Rev. **75**, 1477 (1949).

[37]H. Chermette, Phys. Rev. A **29**, 488 (1984).

[38]F. Herman and S. Skillman, *Atomic Structure Calculations* (Prentice-Hall, Englewood Cliffs, N. J., 1963).

[39]L. Tterlikkis, S. D. Mahanti, and T. P. Das, Phys. Rev. **176**, 10 (1968).

[40]G. W. Brindley and F. E. Hoare, Trans. Faraday Soc. **33**, 268 (1937); Proc. Phys. Soc. London **49**, 619 (1937).

[41]H. Kanazawa and N. Matsudawa, Prog. Theor. Phys. **23**, 433 (1960).

[42]See, for example, V. L. Moruzzi, J. F. Janak, and A. R. Williams, *Calculated Electronic Properties of Metals* (Pergamon, New York, 1978).

[43]J. Yamashita and S. Asano, J. Phys. Soc. Jpn. **29**, 264 (1970).

[44]E. W. Collings, Phys. Kondens. Mater **3**, 335 (1965).

[45]The total susceptibility data of Ref. 44 were adjusted by about 8% to agree in absolute value with those of Ref. 6 in the range where they overlap ($\rho \simeq 1.8$ g cm^{-3}).